# Supporting Information

## Precisely Tailoring d-Band Center of Pt via Metal–Semiconductor Interaction for C1 Small Molecule Electrooxidation

Ya Yan, Qiang Yuan*

State Key Laboratory of Green Pesticide, Center for R&D of Fine Chemicals, College of Chemistry and Chemical Engineering, Guizhou University, Guiyang, Guizhou Province 550025, P. R. China

E-mail: qyuan@gzu.edu.cn.

## Chemicals

Chloroplatinic acid ($K_2PtCl_6 \cdot 6H_2O$, 99.9%) was purchased from Aldrich, Bismuth chloride ($BiCl_3$, AR) and Tellurium oxide ($TeO_2$ ,AR) was purchased from Macklin, Polyvinylpyrrolidone (PVP, P40) and Hydrazine hydrate ($N_2H_4 \cdot H_2O$) were purchased from Aldrich, Sodium hydroxide (NaOH, AR), Ethanol (99.8 %), ethylene glycol (EG, AR), Formic acid (HCOOH, AR), Perchloric acid ($HClO_4$, AR) ,Sulfuric acid ($H_2SO_4$) and Methanol ($CH_3OH$) were purchased from Sinopharm Chemical Reagent Co. Ltd. (Shanghai, China), Pt/C (20 wt% and 60 wt%) catalyst was obtained from Johnson Matthey. Vulcan XC-72 was got from Cabot.

## Synthesis of $Bi_2Te_3$ seeds

In detail, 0.4 g of PVP, 0.315 g of $BiCl_3$, 0.24 g of $TeO_2$ and o.5 g NaOH were added to 22.5 mL of EG and 0.25 mL of $N_2H_4 \cdot H_2O$ and stirred at room temperature for 60 min, to a 50 mL Teflon-lined stainless-steel autoclave. Then, the sealed autoclave was heated at 180 ℃ for 1 h, cooled to room temperature. The product was washed three times with ethanol, and the final product was dispersed in 30 mL of ethanol.

## Synthesis of Pt/$Bi_2Te_3$ with different content

For this synthesis, synthesized via a visible light-assisted template method. 0.5 mL of $Bi_2Te_3$ was added to 10 mL of ethylene glycol, and the mixture was stirred

at 900 rpm. Subsequently, different volumes (700 μL, 800 μL, 900 μL, 1000 μL, and 1100 μL) of 0.01 M $K_2PtCl_6$ were added. The mixture was stirred at room temperature for five minutes and then placed under a 40 W desk lamp equipped with a tungsten wire for 2 hours. The obtained black product was washed and centrifuged with anhydrous ethanol, and finally made up to 4 mL with anhydrous ethanol to yield the final products: Pt/$Bi_2Te_3$-56.1, Pt/$Bi_2Te_3$-56.9, Pt/$Bi_2Te_3$-64.3, Pt/$Bi_2Te_3$-66.1, and Pt/$Bi_2Te_3$-66.8.

**Characterizations**

The morphology was analyzed by TEM (JEM-1400 Flash) and high-resolution high-angle annular dark-field scanning transmission electron microscopy (HAADF-STEM) (FEI, Themis Z). The X-ray diffraction (XRD) patterns of the samples were recorded on a Bruker D8 Advance diffractometer with Cu Kα radiation (λ=1.5418 Å) with graphite monochromator (40 KV, 40 mA). X-ray photoelectron spectroscopy (XPS) was conducted on a Thermo ScientificTM K AlphaTM+ spectrometer equipped with a monochromatic Al Kα X-ray source (1486.6 eV) operating at 100 W. Binding energy was corrected from charge effects by reference to the C1s peak of carbon at 284.8 eV. The inductively coupled plasma optical emission spectrometry (ICP-OES) analysis of samples was performed on iCAP 7200 (ThermoFisher) and determined the compositions. The XAFS data were processed according to the standard procedures using the Athena module implemented in the IFEFFIT software

packages. The EXAFS spectra were obtained by subtracting the post-edge background from the overall absorption and then normalizing with respect to the edge-jump step. Subsequently, the $\chi^{(k)}$ data of were Fourier transformed to real (R) space using a hanning windows (dk = 1.0 $Å^{-1}$) to separate the EXAFS contributions from different coordination shells. To obtain the quantitative structural parameters around central atoms, least-squares curve parameter fitting was performed using the ARTEMIS module of IFEFFIT software packages.

**The computing method of d-band centers**

The d-band centers of corresponding Pt nanocrystal and commercial Pt/C were calculated from the following equation based on the valence band spectra.

$$d-band\ center = \int_{-2eV}^{8eV} [binding\ energy(E)]dE / \int_{-2eV}^{8eV} intensity(E)dE$$

**The computing method of ECSA**

The ECSA of Pt/C were calculated by the following equation:

$$ECSA = \frac{Q_H}{210 \times Pt_m}$$

QH is the charge for Hupd adsorption determined using QH = 0.5×Q, $Pt_m$ is associated with the loading of Pt on the work electrode, and 210 μC $cm^{-2}$ is the charge required for the monolayer adsorption of hydrogen on the Pt surface.

**Electrochemical measurements**

All electrochemical measurements for the FAOR test were performed at room temperature by employing a three-electrode electrochemical cell with an electrochemical workstation (CHI, 760E). The glassy carbon electrode (GC, Φ=5 mm) was employed as the working electrode, along with the carbon rod as the counter electrode and the Ag/AgCl electrode as the reference electrode. The loading mass of the precious metal (Pt metal) recorded by performing ICP-OES on the GC electrodes containing Pt/$Bi_2Te_3$-700, Pt/$Bi_2Te_3$-800, Pt/$Bi_2Te_3$-900, Pt/$Bi_2Te_3$-1000, Pt/$Bi_2Te_3$-1100 and Pt/C was 0.83, 0.86, 0.91, 0.85, 0.87 and 1.0 μg. Before testing, the catalyst was first activated by cycling between 0.01-1.16 V (vs. RHE) in $N_2$ saturated 0.5 M $H_2SO_4$ solution until voltammograms were obtained (30 cycles). Cyclic voltammetry (CV) curve was subsequently obtained under the same testing conditions. Formic acid oxidation was conducted in $N_2$-saturated 0.5 M $H_2SO_4$ + 3 M HCOOH, and methanol oxidation was conducted in $N_2$-saturated 1 M KOH + 1 M $CH_3OH$, at a scan rate of 50 mV $s^{-1}$. Long-term stability test was performed by chronoamperometry at 0.5 V vs. RHE for 3 h in $N_2$-saturated 0.5 M $H_2SO_4$ containing 3 M HCOOH (FAOR) or 1 M KOH containing 1 M $CH_3OH$ (MOR). To evaluate the CO poisoning tolerance ability for each catalyst, In situ anti-CO performance were carried out as follows. Initially, the stable catalytic activity was measured in 0.5 M $H_2SO_4$ + 3 M HCOOH as the reference CV curve. The in situ anti-CO poisoning experiments were carried out in 0.5 M

$H_2SO_4$ + 3 M HCOOH solution. Before performing CVs, CO gas was first inputted with a flow rate of 15 mL $min^{-1}$ for 5 min, then kept CO inputting and CV scanning was performed. Similarly, the in situ CO resistance performance test for methanol oxidation was conducted in 1 M KOH + 1 M $CH_3OH$.

**In situ ATR-SEIRAS measurements**

In situ attenuated total reflectance-surface enhanced infrared absorption spectroscopy (in situ ATR-SEIRAS) reflection spectroscopy was conducted on a Nicolet-iS50 FT-IR spectrometer containing a liquid nitrogen-cooled MCT-A detector, at a spectral resolution of 8 $cm^{-1}$. The species (absorbed and dissolved) on an A u-coated silicon prism was electrochemically cleaned until stable in Ar-saturated 0.5 M $H_2SO_4$+3 M HCOOH solution. Multi-stepped FTIR spectroscopy (MS-FTIR) was utilized to collect spectra in 0.5 M $H_2SO_4$ + 3 M HCOOH electrolytes from 0.1 to 1.1 V (vs. RHE) at 0.1 V intervals. The relative change in reflectivity (ΔR/R) of spectra was calculated by the following equation:

$$\Delta R = \frac{R(E_S) - R(E_R)}{R(E_R)}$$

Where $R(E_S)$ and $R(E_R)$ are single-beam spectra collected at the sample potential $E_S$ and reference potential $E_R$.

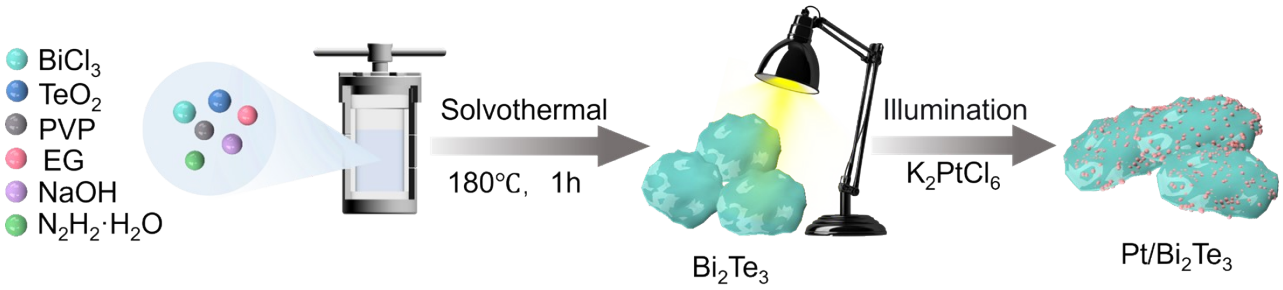


**Figure S1.** Schematic illustration of the synthesis process of $Pt/Bi_2Te_3$ nanosheets.

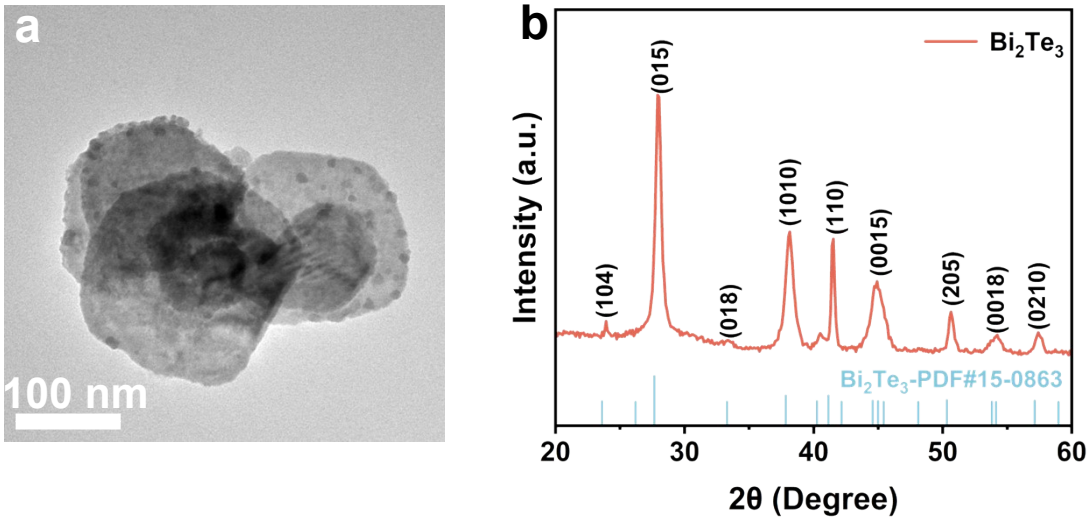


**Figure S2.** (a) TEM, (b) XRD patterns of $Bi_2Te_3$.

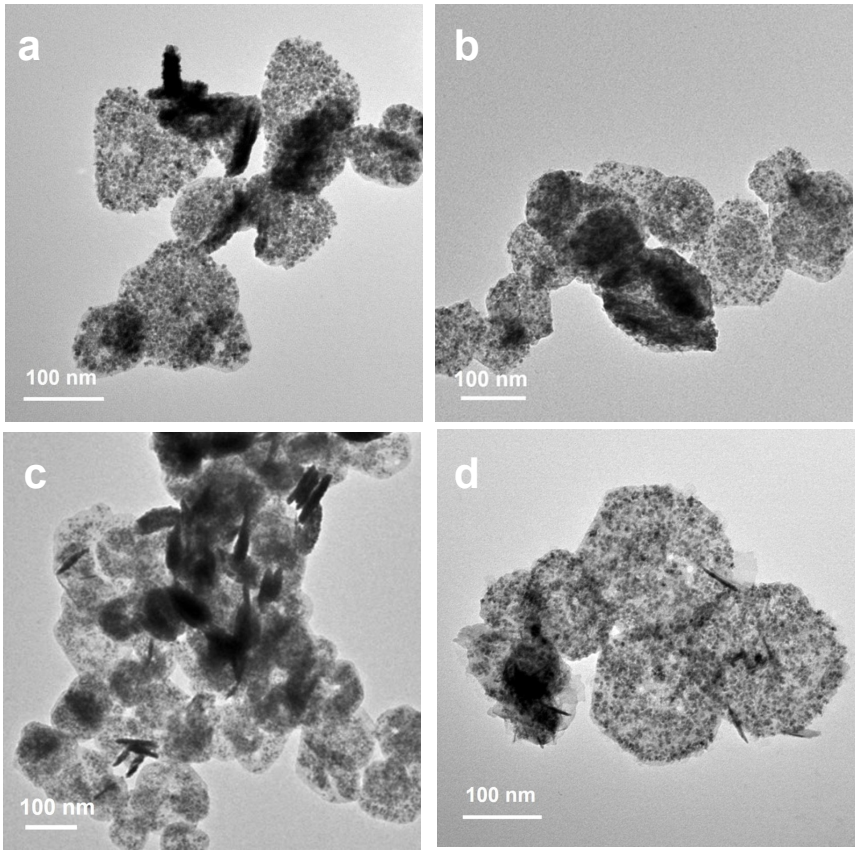


**Figure S3.** TEM images of $Pt/Bi_2Te_3$ with different contents: (a) $Pt/Bi_2Te_3$-56.1, (b) $Pt/Bi_2Te_3$-56.9, (c) $Pt/Bi_2Te_3$-66.1, (d) $Pt/Bi_2Te_3$-66.8.

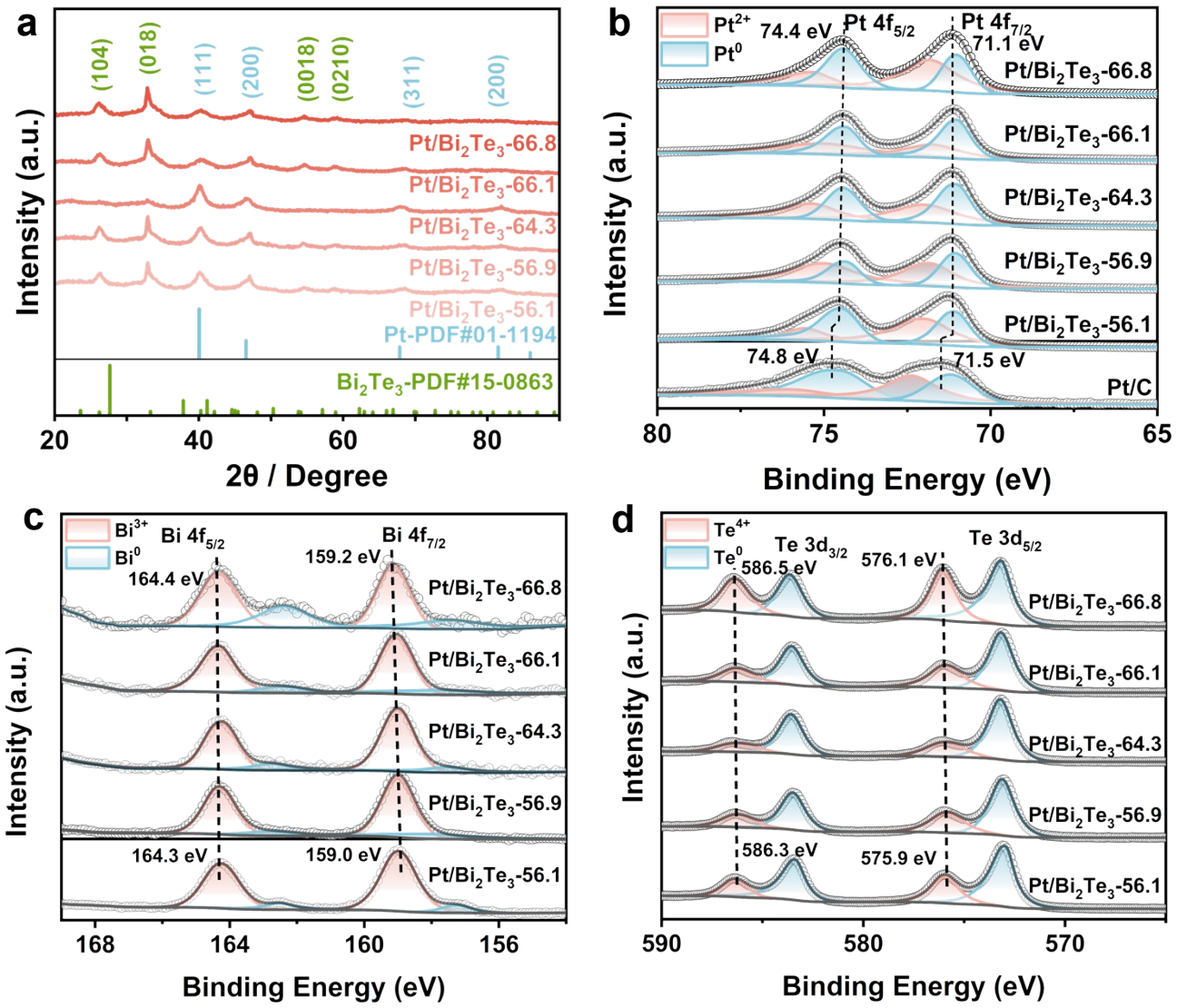


**Figure S4.** (a) $Pt/Bi_2Te_3$ with different contents of XRD patterns. XPS spectra of commercial Pt/C and $Pt/Bi_2Te_3$ with different contents: (b) Pt 4f, (c) Bi 4f, (d) Te 3d.

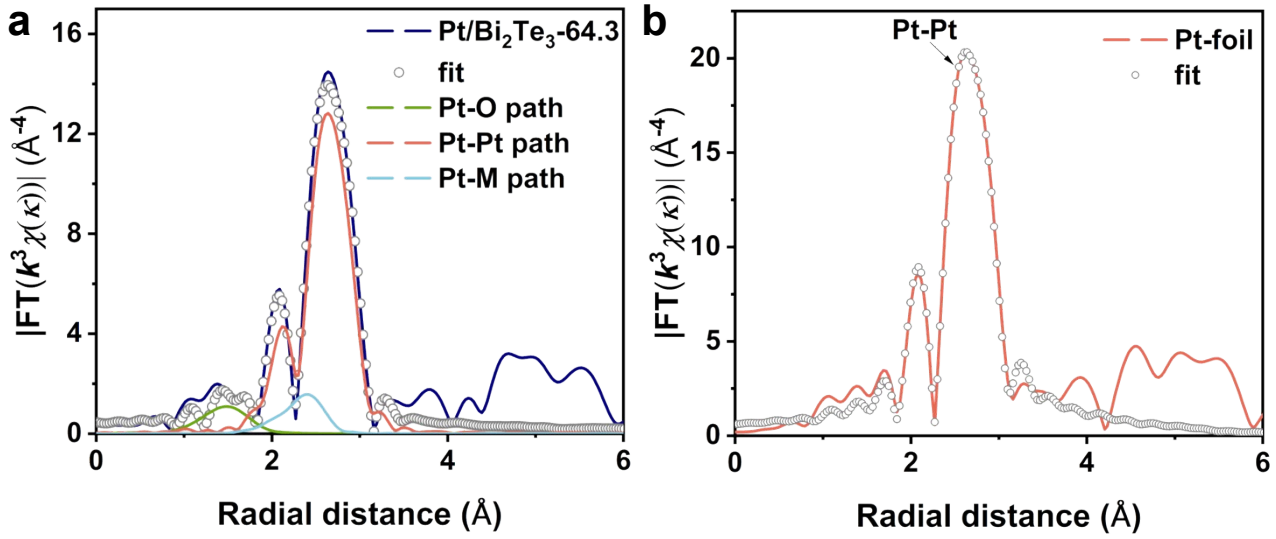


**Figure S5.** Pt $L_3$-edge EXAFS fitting of (a) $Pt/Bi_2Te_3$-64.3, (b) Pt-foil.

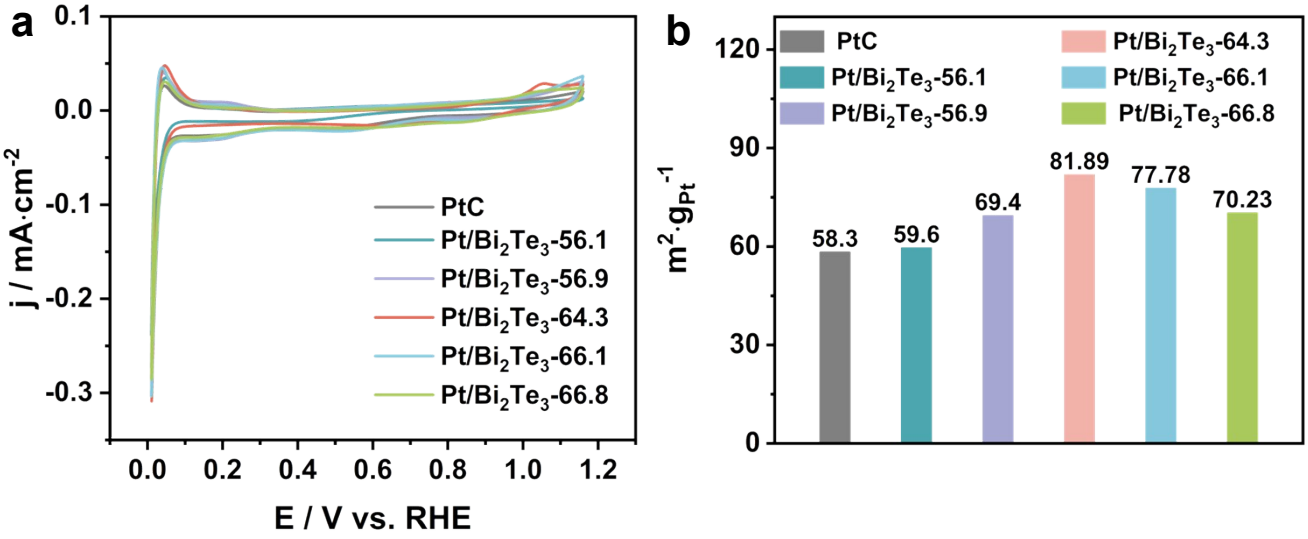


**Figure S6.** (a) CV curves of different catalysts in 0.5 M $H_2SO_4$, (b) ECSA of different catalysts and commercial Pt/C.

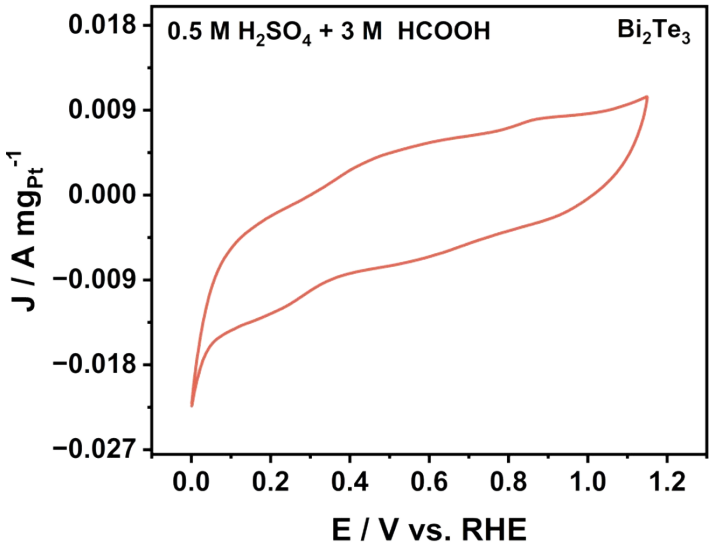


**Figure S7.** CV curves of $Bi_2Te_3$ in 0.5 M $H_2SO_4$ and 3 M HCOOH.

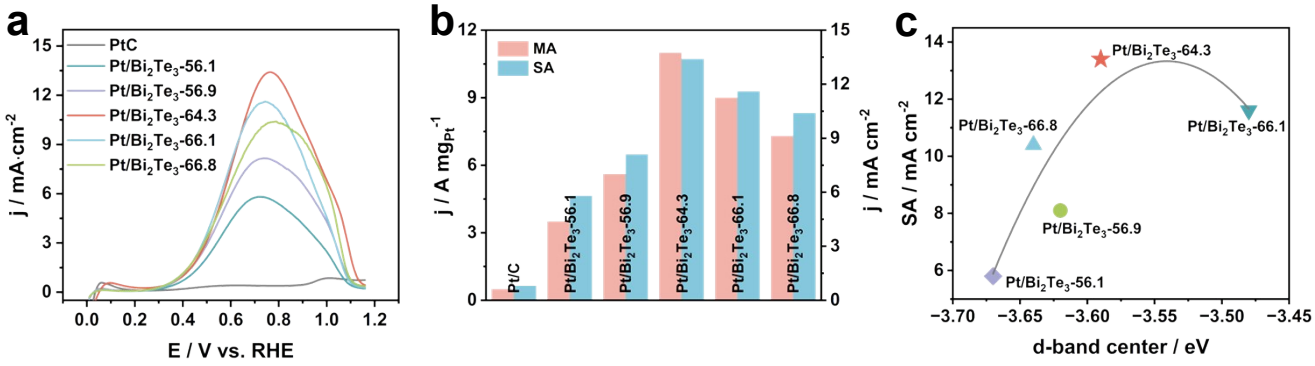


**Figure S8.** (a) CV curves of $Pt/Bi_2Te_3$ and commercial Pt/C in 0.5 M $H_2SO_4$ and 3 M HCOOH. (b) comparison of MA and SA, (c) Volcano-like plot between specific activity (SA) and d-band center.

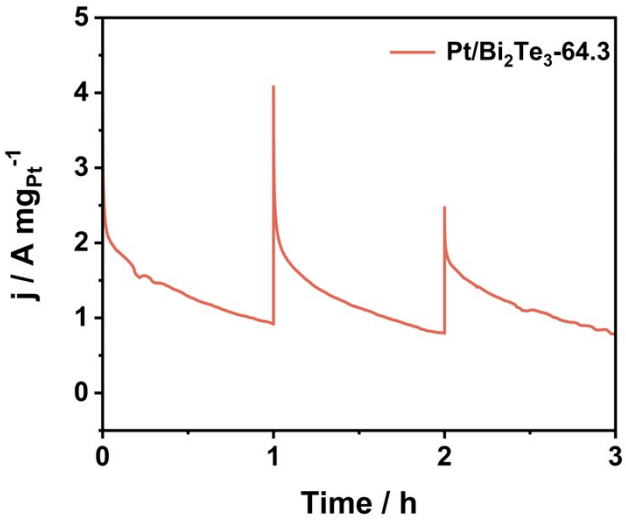


**Figure S9.** Current-time test curves of $Pt/Bi_2Te_3$-64.3 in 0.5 M $H_2SO_4$ + 3 M CHOOH.

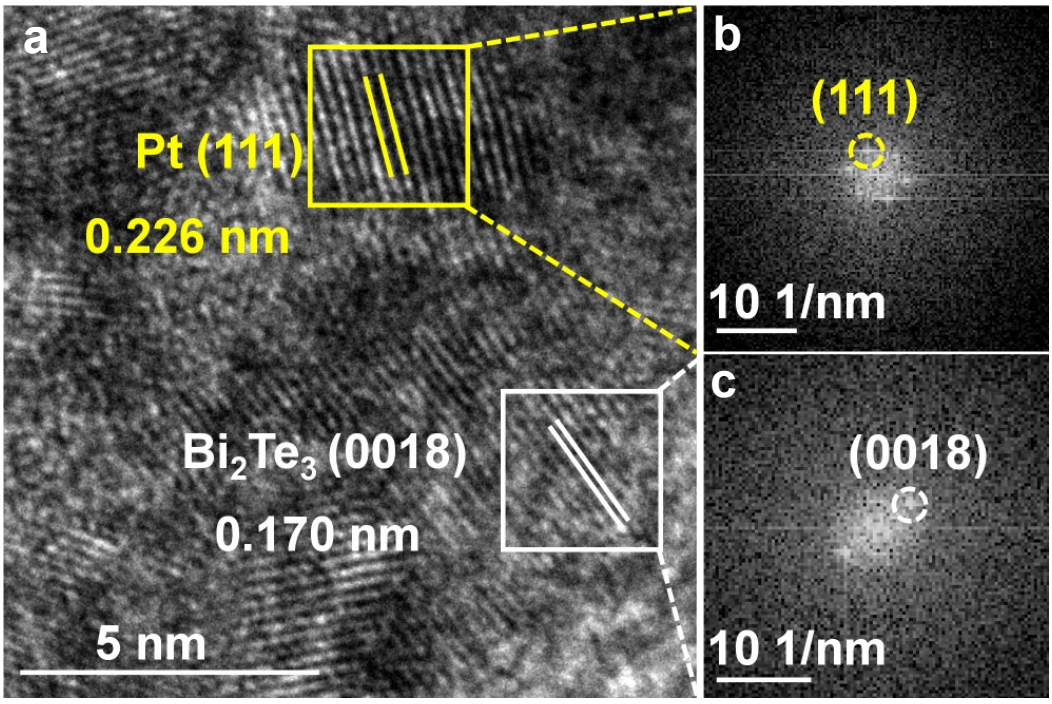


**Figure S10.** (a) HRTEM images and (b, c) the corresponding FFT images of $Pt/Bi_2Te_3$-64.3 after a 3 h stability test for FAOR.

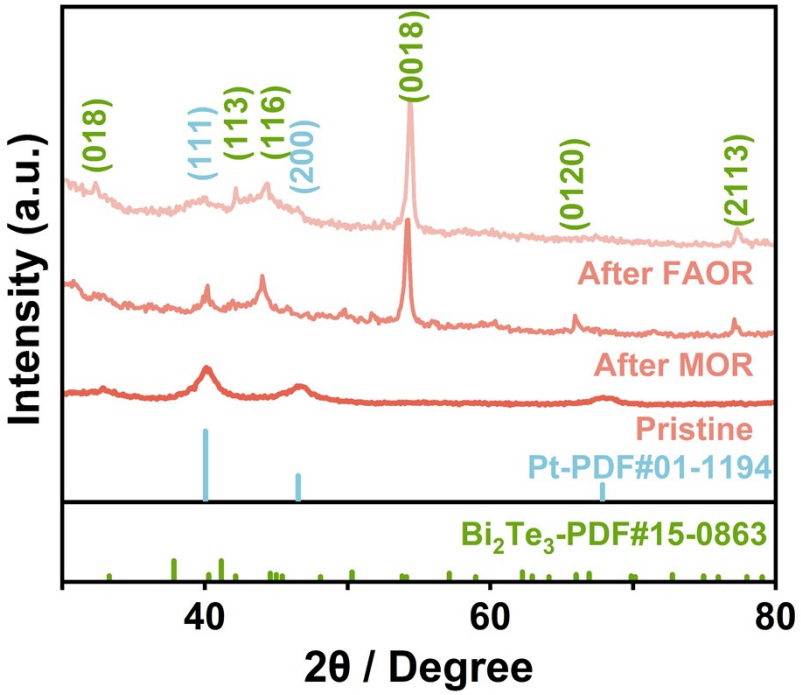


**Figure S11.** XRD patterns of Pt/$Bi_2Te_3$-64.3 after 3 h FAOR/MOR stability test.

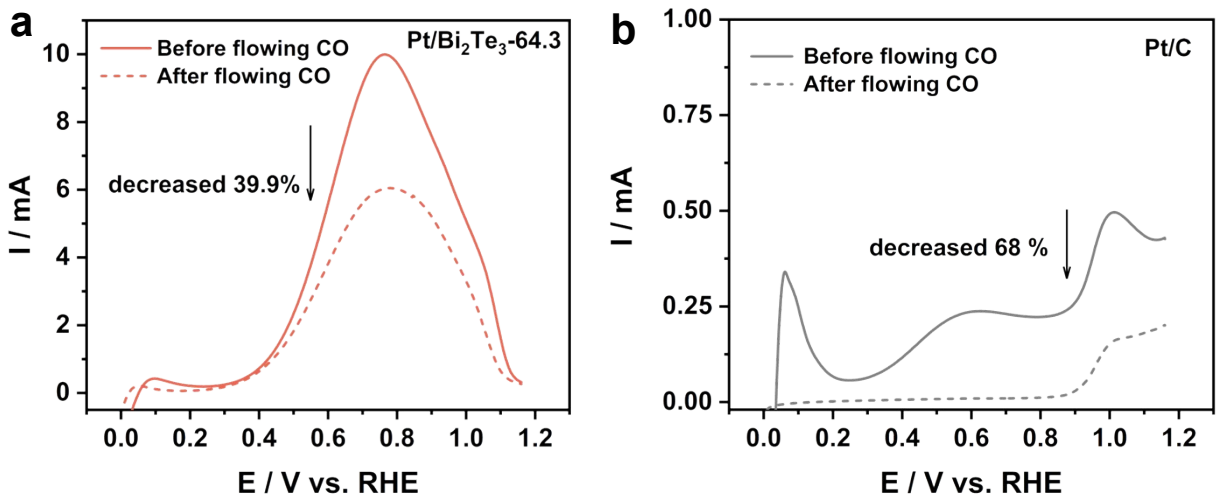


**Figure S12.** In situ CO tests of Pt/$Bi_2Te_3$-64.3 and commercial Pt/C in 0.5 M $H_2SO_4$ and 3 M HCOOH.

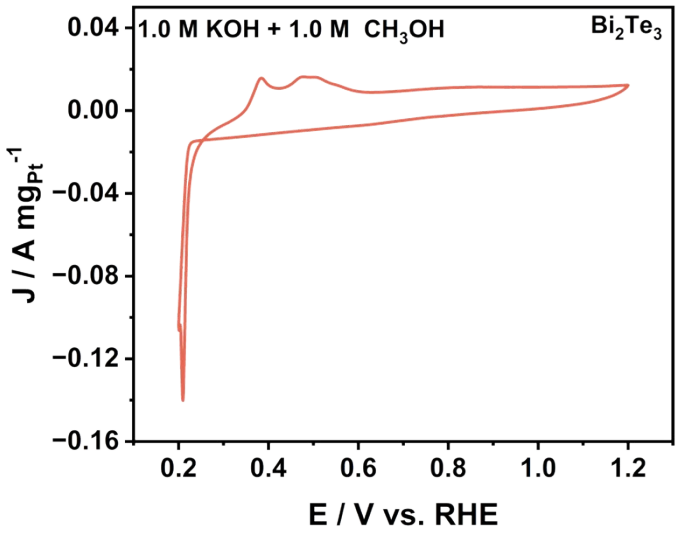


**Figure S13.** CV curves of $Bi_2Te_3$ in 1.0 M KOH and 1 M $CH_3OH$.

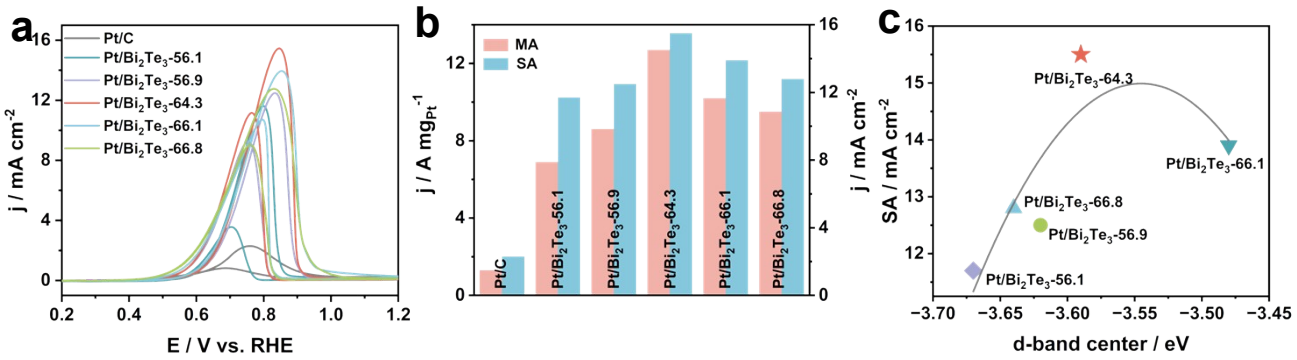


**Figure S14.** (a) CV curves of $Pt/Bi_2Te_3$ and commercial Pt/C in 1.0 M KOH and 1 M $CH_3OH$. (b) comparison of MA and SA, (c) Volcano-like plot between specific activity (SA) and d-band center.

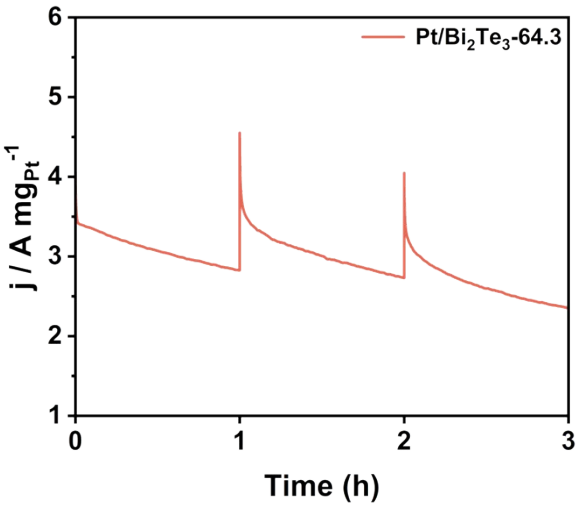


**Figure S15.** Current-time test curves of $Pt/Bi_2Te_3$-64.3 in 1.0 M KOH + 1.0 M $CH_3OH$.

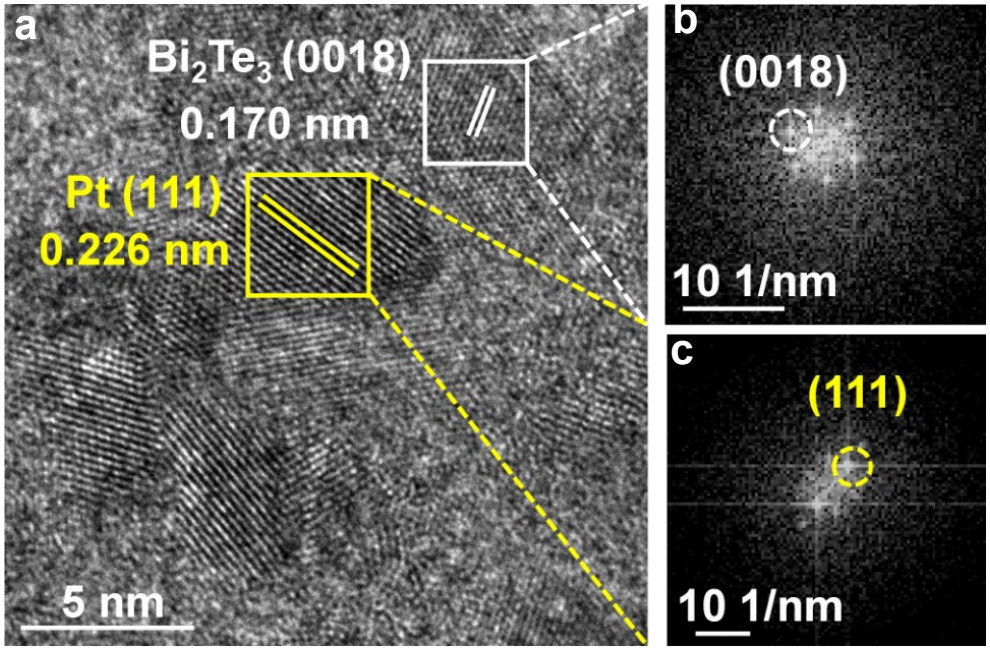


**Figure S16.** (a) HRTEM images and (b, c) the corresponding FFT images of $Pt/Bi_2Te_3$-64.3 after a 3 h stability test for MOR.

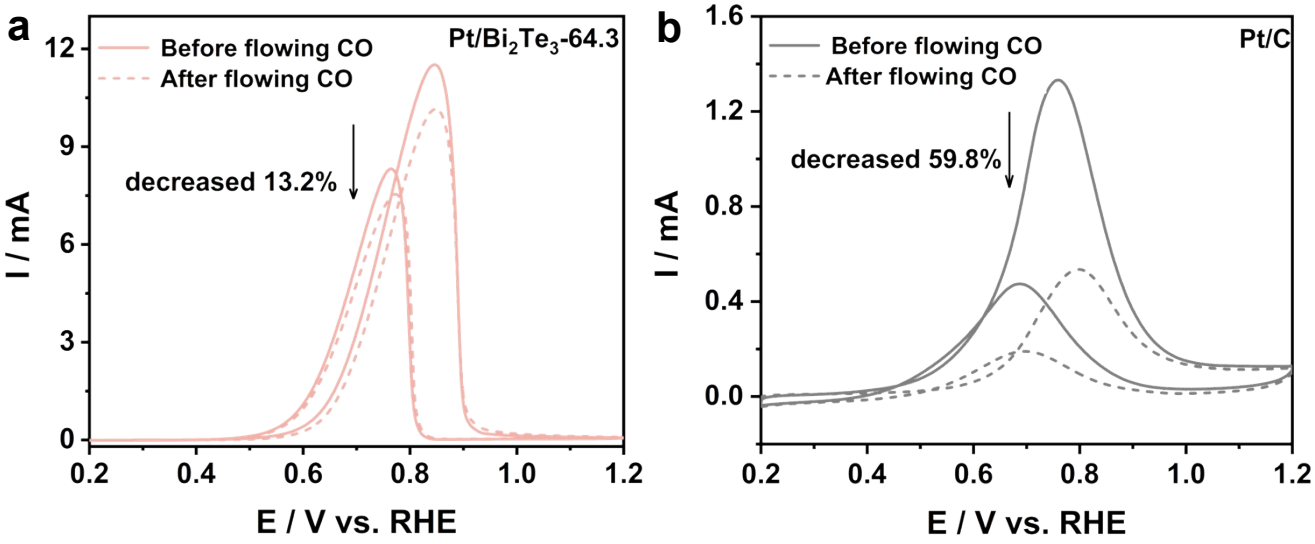


**Figure S17.** In situ CO tests of $Pt/Bi_2Te_3$-64.3 and commercial Pt/C in 1 M KOH and 1 M $CH_3OH$.

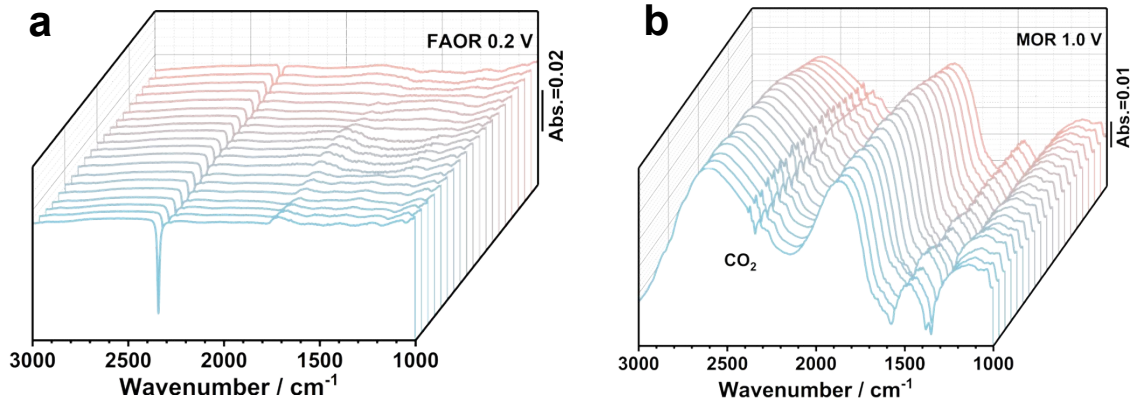


**Figure S18.** $Pt/Bi_2Te_3$-64.3 (a) in 0.5 M $H_2SO_4$ and 3 M HCOOH in situ ATR-SEIRAS at 1.0 V with 2 s intervals; (b) in1.0 M KOH and 1.0 M $CH_3OH$ in situ FTIR at 1.0 V with 2 s intervals.

**Table S1** ICP-OES test results of $Bi_2Te_3$ and $Pt/Bi_2Te_3$ with different contents.

| | ICP-OES |
|---|---|
| $Bi_2Te_3$ | Bi/Te = 40.96/59.04 |
| $Pt/Bi_2Te_3$-56.1 | Pt//Bi/Te = 48.96/11.73/39.31 |
| $Pt/Bi_2Te_3$-56.9 | Pt//Bi/Te = 49.7/11.5/38.8 |
| $Pt/Bi_2Te_3$-64.3 | Pt//Bi/Te = 55.23/6.19/38.58 |
| $Pt/Bi_2Te_3$-66.1 | Pt//Bi/Te = 57.78/5.17/37.05 |
| $Pt/Bi_2Te_3$-66.8 | Pt//Bi/Te = 58.11/4.02/37.87 |

**Table S2** XPS valence state ratios of $Pt/Bi_2Te_3$ samples with different Pt loadings.

| Sample | $Pt^{2+}/Pt^0$ | $Bi^{3+}/Bi^0$ | $Te^{4+}/Te^0$ |
|---|---|---|---|
| $Pt/Bi_2Te_3$-56.1 | 0.91 | 5.33 | 0.58 |
| $Pt/Bi_2Te_3$-56.9 | 1.07 | 5 | 0.48 |
| $Pt/Bi_2Te_3$-64.3 | 0.99 | 4.5 | 0.48 |
| $Pt/Bi_2Te_3$-66.1 | 1.15 | 1.75 | 0.23 |
| $Pt/Bi_2Te_3$-66.8 | 0.91 | 7.1 | 0.78 |

**Table S3** XAFS fitting parameters at the Pt $L_3$-edge for various samples.

| Sample | Path | *CN*[a] | *R*(Å)[b] | $\sigma^2$ (Å$^2$)[c] | $\Delta E_0$(eV)[d] | *R* factor |
|---|---|---|---|---|---|---|
| Pt $L_3$-edge ($S_0^2$=0.860) | | | | | | |
| Pt foil | Pt-Pt | 12.0* | 2.760±0.002 | 0.0046 | 6.6±0.7 | 0.0042 |
| $Pt/Bi_2Te_3$-64.3 | Pt-O | 0.7±0.5 | 1.825±0.012 | 0.0147 | 7.7±1.6 | 0.0122 |
| | Pt-M | 0.6±0.3 | 2.601±0.005 | 0.0055 | | |
| | Pt-Pt | 11.4±0.2 | 2.765±0.023 | | | |

[a]*CN*, coordination number; [b]*R*, the distance between absorber and backscatter atom s; [c]$\sigma^2$, the Debye Waller factor value; [d]$\Delta E_0$, inner potential correction to account for the difference in the inner potential between the sample and the reference compound; *R* factor indicates the goodness of the fit.

**Table S4** FAOR mass activity of reported Pt-based catalysts.

| Catalysts | Electrolyte | Mass activity ($A\ mg^{-1}$) | Specific activity ($mA\ cm^{-2}$) | Reference |
|---|---|---|---|---|
| $Pt/Bi_2Te_3$-64.3 | 0.5 M $H_2SO_4$+3 M HCOOH | 11.0 | 13.4 | This work |
| PtBiPbNiCo | 0.5 M H2SO4 +0.5 M HCOOH | 7.1 | 27.2 | 1 |
| PtPbBi/PtBi NPs | 0.5 M $H_2SO_4$+0.5 M HCOOH | 7.4 | 25.1 | 2 |
| PtIrBi NPs/C | 0.1 M $HClO_4$+0.5 M HCOOH | 8.2 | 18.2 | 3 |
| (Y-Pt)-$PtTe_2$ HPNT/C | 0.5 M $H_2SO_4$+0.5 M HCOOH | 6.4 | 5.4 | 4 |
| Pt-PbS NBs/C | 0.5 M $H_2SO_4$+0.5 M HCOOH | 5.9 | 21.4 | 5 |
| PtPdAg NTs | 0.5 M $H_2SO_4$+0.5 M HCOOH | 1.65 | 3.73 | 6 |
| Pd@Pt/C SAA | 0.1 M $HClO_4$+2 M HCOOH | 5.2 | - | 7 |
| Pt-ALs/CrN | 0.1 M $HClO_4$+1 M HCOOH | 5.17 | - | 8 |
| PtBi@1.8% Pd HNPs | 0.5 M $H_2SO_4$+1 M HCOOH | 4.17 | - | 9 |
| $Au_{6.4}Ag_{2.6}Pt_{1.0}$-NWs | 0.5 M $H_2SO_4$+0.5 M HCOOH | 3.081 | - | 10 |
| Au-Pt | 0.5 M $H_2SO_4$+0.5 M HCOOH | 1.94 | 7.89 | 11 |
| m-$PtTe_2$ NT | 0.5 M $H_2SO_4$+0.5 M HCOOH | 3.2 | 6.78 | 12 |

**Table S5** MOR mass activity of reported Pt-based catalysts.

| Catalysts | Electrolyte | Mass activity ($A\ mg^{-1}$) | Specific activity ($mA\ cm^{-2}$) | Reference |
|---|---|---|---|---|
| $Pt/Bi_2Te_3$-64.3 | 1 M KOH + 1 M $CH_3OH$ | 12.7 | 15.5 | This work |
| PdAgSn/PtBi HEA NPs | 1 M KOH + 1 M $CH_3OH$ | 2.847 | 4.7 | 13 |
| PtBr NPs/Br-GDY | 1 M KOH + 0.5 M $CH_3OH$ | 10.4 | 17.4 | 14 |
| Co-N-C-100/Pt | 1 M KOH + 3 M $CH_3OH$ | 5.8 | 10.8 | 15 |
| PPt NDs | 1 M KOH + 1 M $CH_3OH$ | 4.2 | 17.3 | 16 |
| $Pt_{1.8}Pd_{0.2}CuGa$ | 1 M KOH + 1 M $CH_3OH$ | 11.13 | 18.13 | 17 |
| $Pt_3Yb/C$ | 1 M KOH + 1 M CH3OH | 11.61 | 35.28 | 18 |
| $Ptc/Ti_3C_2T_x$ | 1 M KOH + 1 M $CH_3OH$ | 7.32 | 38 | 19 |
| Pt/La-MoC | 1 M KOH + 0.5 M $CH_3OH$ | 8.58 | - | 20 |
| $Pt\text{-}SrRuO_3/RuO_2$ | 1 M KOH + 1 M $CH_3OH$ | 4.88 | - | 21 |
| $Pt_{78}La_{22}/C$ | 1 M KOH + 1 M $CH_3OH$ | 4.44 | - | 22 |
| GDY/Vo-PtOxCc | 1 M KOH + 1 M $CH_3OH$ | 8.8 | - | 23 |
| Pt@NiCo-LDH | 1 M KOH + 3 M $CH_3OH$ | 2.57 | 232.71 | 24 |

## References


1. C. Zhan, L. Bu, H. Sun, X. Huang, Z. Zhu, T. Yang, H. Ma, L. Li, Y. Wang, H. Geng, W. Wang, H. Zhu, C. W. Pao, Q. Shao, Z. Yang, W. Liu, Z. Xie and X. Huang, Angew. Chem. Int. Ed., 2022, **62**, e202213783
2. X. Hu, Z. Xiao, W. Wang, L. Bu, Z. An, S. Liu, C.-W. Pao, C. Zhan, Z. Hu, Z. Yang, Y. Wang and X. Huang, J. Am. Chem. Soc., 2023, **145**, 15109-15117.
3. Y. Sun, W. Chen, W. Zhang, Y. Nie, Q. Zhang, L. Gu, M. Luo and S. Guo, Adv. Funct. Mater., 2023, **33**, 2303299.
4. X. Lin, S. Geng, X. Du, F. Wang, X. Zhang, F. Xiao, Z. Xiao, Y. Wang, J. Cheng, Z. Zheng, X. Huang and L. Bu, Nat. Commun., 2025, **16**, 147.
5. L. Liu, L. Jin, Z. Xiao, N. Fang, X. Lin, Y. Ji, Y. Wang, Y. Li, X. Huang and L. Bu, Nano Lett., 2024,

**24**, 8162-8170.
6. Y. F. Wang, S. L. Zhang, Y. X. Deng, S. H. Luan, C. K. Wang, L. F. Ding, X. Jiang, D. M. Sun and Y. W. Tang, Rare Met., 2024, **44**, 300-310.
7. J. Li, X. Liang, L. Cai, S. Huang and C. Zhao, ACS Appl. Mater. Interfaces, 2022, **14**, 8001-8009.
8. R. Feng, D. Li, H. Yang, C. Li, Y. Zhao, G. I. N. Waterhouse, L. Shang and T. Zhang, Adv. Mater., 2023, **36**, 2309251.
9. M. Tang, W. Chen, S. Luo, X. Wu, X. Fan, Y. Liao, X. Song, Y. Cheng, L. Li, L. Tan, Y. Liu and Z. Quan, J. Mater. Chem. A, 2021, **9**, 9602-9608.
10. Z.-N. Zhang, X.-H. Wang, X.-L. Tian, Y. Chen and S.-N. Li, J. Mater. Chem. A, 2023, **11**, 21628-21635.
11. X. Li, J. Zhang, C. Jin, B. Yan, J. Cai, M. Li, X. Peng and Y. Wang, ACS Sustain. Chem. Eng., 2021, **9**, 11062-11069.
12. C. Dong, B. Zhang, H. Song, S. Zhou, J. Ye, H.-G. Liao, L. Dong, X. Huang and L. Bu, ACS Nano, 2024, **18**, 10008-10018.
13. X. Lao, X. Liao, C. Chen, J. Wang, L. Yang, Z. Li, J. W. Ma, A. Fu, H. Gao and P. Guo, Angew. Chem. Int. Ed., 2023, **62**, e202304510.
14. L. Hui, D. Yan, X. Zhang, H. Wu, J. Li and Y. Li, Angew. Chem. Int. Ed., 2024, 63, e202410413.
15. J. Ruan, Y. Chen, G. Zhao, P. Li, B. Zhang, Y. Jiang, T. Ma, H. Pan, S. X. Dou and W. Sun, Small, 2022, **18**, 2107067.
16. K. Guo, D. Fan, J. Bao, Y. Li and D. Xu, Adv. Funct. Mater., 2022, **32**, 2208057.
17. K. Xu, L. Liang, T. Li, M. Bao, Z. Yu, J. Wang, S. M. Thalluri, F. Lin, Q. Liu, Z. Cui, S. Song and L. Liu, Adv. Mater., 2024, **36**, 2403792.
18. S. Zhang, L. Yin, Q. Liu, G. Hai and Y. Du, ACS Nano, 2024, **18**, 25754-25764.
19. J. Zhu, L. Xia, R. Yu, R. Lu, J. Li, R. He, Y. Wu, W. Zhang, X. Hong, W. Chen, Y. Zhao, L. Zhou, L. Mai and Z. Wang, J. Am. Chem. Soc., 2022, **144**, 15529-15538.
20. W. Wei, X. Peng, Q. Zhou, M. Wang, H. Tang, J. Xie, S. Tian, W. Zhou, X. Ren and D. Ma, J. Am. Chem. Soc., 2025, **147**, 38465-38474.
21. Z. Zeng, J. Long, Z. Zhou, Y. Chen, J. Huang and X. Wu, Chem. Eng. J., 2025, **522**, 167785.
22. Y. Feng, S. Zhang, M. Chen, L. Zhu, A. Pei, F. Wu, X. Liao, Q. Gao, W. Wang, Z. Yang, H. Ye and B. H. Chen, J. Colloid Interface Sci., 2025, **679**, 918-928.
23. X. Zhang, L. Hui, Z. Wang, C. Liu, Y. Yang and Y. Li, J. Am. Chem. Soc., 2026, **148**, 2995-3005.
24. B. Zhu, J. Xiong, S. Wu, B. Sun, Y. Liu, Y. Zhang, H. Lin, Z. Wu and L. Feng, Angew. Chem. Int. Ed., 2026, **65**, e25802.